Acidic Effect of Porous Alumina as Supports for Pt Nanoparticle Catalysts in n-Hexane Reforming

Journal:	*Catalysis Science & Technology*
Manuscript ID	CY-ART-04-2018-000776.R1
Article Type:	Paper
Date Submitted by the Author:	18-May-2018

Complete List of Authors:	Yang, Euiseop; Ulsan National Institute of Science and Technology, School of Energy and Chemical Engineering Jang, Eun Jeong; Ulsan National Institute of Science and Technology, School of Energy and Chemical Engineering Lee, Jun Gyeong; Ulsan National Institute of Science and Technology, School of energy and chemical engineering Yoon, Sinmyung; Ulsan National Institute of Science and Technology, School of Energy and Chemical Engineering Lee, Jaekyoung; Ulsan National Institute of Science and Technology, School of Energy and Chemical Engineering Musselwhite, Nathan; University of California, Berkeley, Department of Chemistry Somorjai, Gabor; University of California at Berkeley, Chemistry Kwak, Ja Hun; UNIST, Chemical Engineering An, Kwangjin; UNIST, School of Energy and Chemical Engineering

Journal Name

ARTICLE

Acidic Effect of Porous Alumina as Supports for Pt Nanoparticle Catalysts in *n*-Hexane Reforming

Received 00th January 20xx,
Accepted 00th January 20xx

DOI: 10.1039/x0xx00000x

www.rsc.org/

Euiseob Yang,†[a] Eun Jeong Jang,†[a] Jun Gyeong Lee,[a] Sinmyung Yoon,[a] Jaekyoung Lee,[a] Nathan Musselwhite,[b,c] Gabor A. Somorjai,[b,c] Ja Hun Kwak,*[a] and Kwangjin An*[a]

Acidic halogen-modified (Cl and F) porous alumina supports with well-defined macropores and mesopores were designed to prepare alumina-supported Pt nanoparticle (NP) catalysts (Pt/Cl-Al_2O_3, Pt/F-Al_2O_3, and Pt/Al_2O_3). The catalysts were then used for *n*-hexane reforming in a tubular fixed bed reactor with a hexane:H_2 ratio of 1:4.3 at ambient pressure and various temperatures (240–400 °C). Although the reaction rates for all catalysts were maximised at 360 °C, Pt/Cl-Al_2O_3 exhibited the highest rate (at 8.66 × 10^{-8} mol/s). Regarding product selectivity, Pt/Cl-Al_2O_3 and Pt/F-Al_2O_3 yielded a higher number of olefin products and fewer cracking products than Pt/Al_2O_3. Temperature programmed desorption (TPD) with ethanol and *in-situ* diffuse-reflectance infrared spectroscopy (DRIFTS) with CO and pyridine adsorption were used to characterise the alumina support surface acidities. Compared with γ-Al_2O_3, the TPD results indicated that the Cl-Al_2O_3 and F-Al_2O_3 surface acidities were enhanced by surface modification. The *in-situ* DRIFTS experiments confirmed that the relative ratio of Lewis to Brønsted acid sites of Cl-Al_2O_3 (0.64) was higher than those of F-Al_2O_3 (0.54) and unmodified Al_2O_3 (0.56). Additionally, the DRIFTS spectra confirmed that the Pt NPs were preferentially deposited to the Lewis acid sites of the supports, and the CO adsorption spectra revealed that Pt NPs with (111) facets were preferentially deposited to the Lewis acid sites. The surface acidity studies indicated that the enhanced Lewis acidity of Cl-Al_2O_3 induced high reaction rates at all temperatures, resulting in skeletal rearrangements of hydrocarbons toward branched isomers at high temperature via a conventional bi-functional mechanism.

Introduction

Catalytic reforming of hydrocarbons has attracted considerable attention because of its practical applications in the petrochemical industry by producing high octane gasoline and many other useful chemicals.[1–4] It is well known that the incorporation of Pt metals into alumina supports or zeolites in naphtha reforming processes leads to bi-functional catalysts, in which Pt and the acidic centres of the supports (either alumina or zeolite) perform different functions.[5–7] Specifically, Pt is responsible for hydrogenation/dehydrogenation of the attached hydrocarbons, whereas the acidic centres induce their skeletal rearrangements. With the remarkable advancements in nanochemistry, well-defined noble metal nanoparticles (NPs) and high-surface porous materials with ordered pore structures have been combined to produce supported nanocatalysts with enhanced catalytic activity, selectivity, and stability beyond the catalysts currently utilised in industrial reforming processes.[8–11]

Recently, composition-controlled bimetallic PtRh NPs supported on mesoporous silica were used for *n*-hexane reforming, since Pt atoms associated with a small amount of another metal (such as Rh, Ir, or Sn) can affect both selectivity and activity.[12] Using this strategy, it was demonstrated that $Pt_{90}Rh_{10}$ NPs with a 93:7 Pt:Rh surface composition exhibited the highest C_6 isomer yield in the *n*-hexane reforming process relative to other compositions examined. This result was attributed to a surface ensemble effect in which C-H bond activation became favoured as the activities of the surface Pt atoms were diluted by highly active Rh atoms. The effects of the support in *n*-hexane reforming have also been studied using other Pt NP systems.[12–16] For example, Pt NPs have been loaded onto different macro-/meso-porous materials (e.g. Al_2O_3, TiO_2, Nb_2O_5, Ta_2O_5, and ZrO_2). Product selectivity toward C_6 isomers was shown to be maximised over the Pt/Nb_2O_5 and Pt/Ta_2O_5 catalysts as a result of their strong metal–support interactions.[13] In addition, the Lewis and Brønsted acid sites of mesoporous silica modified with an aluminium support (Al-MCF-17) were examined for their Pt loading ability during the reforming reaction.[14] Compared with the non-modified MCF-17 supported Pt catalysts (Pt/MCF-17) and pure Al-MCF-17, the modified Pt/Al-MCF-17 catalysts showed a greatly

[a]School of Energy and Chemical Engineering, Ulsan National Institute of Science and Technology(UNIST), Ulsan 44919, Republic of Korea. E-mail: jhkwak@unist.ac.kr, kjan@unist.ac.kr
[b]Department of Chemistry, University of California, Berkeley, CA 94720, United States
[c]Chemical Sciences and Materials Sciences Divisions, Lawrence Berkeley National Laboratory, Berkeley, CA 94720, United States
† These authors contributed equally to this work.
Electronic Supplementary Information (ESI) available: [details of any supplementary information available should be included here]. See DOI: 10.1039/x0xx00000x

enhanced reaction rate and high isomer selectivity for *n*-hexane reforming due to the higher acidity of the modified support. The conventional bi-functional mechanism noted earlier was determined to be operative in this case. Similar studies have also been reported with state-of-the-art zeolites (e.g. mesoporous zeolite type BEA and MFI).[15] Although Pt-supported zeolite catalysts such as BEA/Pt and MFI/Pt yielded high activity for *n*-hexane reforming, mesoporous BEA and MFI produced many undesirable cracking products because the Brønsted acid sites on their surfaces were too strong. Recently, Pt@SiO_2 and Pt@TiO_2 core@shell-type catalysts with mesoporous shells were investigated to determine their thermal stability during high-temperature *n*-hexane reforming.[16] In this case, the results were also consistent with the bi-functional mechanism of industrial reforming catalysts. Given the costs associated with the catalysts, process engineering, and recycling, Pt with a small amount of metal promoters supported on chlorinated alumina catalysts is likely to function as effective industrial reforming catalysts.[17–21] Indeed, Pt on chlorinated alumina catalysts is utilised extensively in naphtha reforming, because alumina has a high thermal stability and moderate acidity following chlorination.

Following the incorporation of halogen atoms into alumina supports, the resultant catalytic performances were found to be significantly affected by the surface acidic properties of the supports.[22–33] The hydroxyl groups of the alumina were replaced by Cl or F, which increased the materials' electronegativity and thus heightened the acidity of the remaining hydroxyl groups.[22] For chlorination and fluorination of alumina, several approaches have been investigated.[22–33] Chlorinated alumina supports were prepared from γ-Al_2O_3 by reacting with chlorinating agents such as tetrachloromethane, chloric acid, chloroform, and chlorobenzene at various temperatures.[23–29] When the alumina was treated with HCl at 300–700 °C, hydroxyl groups of the aluminas were substituted by Cl atoms; additional HCl dissociated to Al-O sites and created new OH-groups bearing Brønsted acids.[23] However, Primet and co-workers reported that γ-Al_2O_3 treated with CCl_4 had stronger Lewis acid sites than those of HCl- or $AlCl_3$-treated γ-Al_2O_3. They demonstrated that γ-Al_2O_3 with strong Lewis acidity by chlorine incorporation was responsible for the activity enhancement in *n*-butane isomerization.[24] Further, Cornet et al. reported that Cl-Al_2O_3 treated with HCl at 527 °C enhanced catalytic alkylation, whereas Al_2O_3 reacted with CCl_4 was found to be inefficient for this purpose.[23] Depending on the chlorinating agents and chlorination temperatures, the acidic properties of alumina supports and their corresponding catalytic behaviours varied widely. For fluorinated alumina supports, impregnation with an ammonium fluoride solution is a widely used method.[30–33]

In this study, halogen-modified (Cl and F) porous alumina supports and their corresponding Pt/Al_2O_3 nanocatalysts were designed to investigate the role of acidity in *n*-hexane reforming. Porous aluminas with well-ordered macro- and meso-structures were treated with HCl or NH_4F to generate Cl-Al_2O_3 and F-Al_2O_3, respectively, and uniformly sized Pt NPs were incorporated into the modified aluminas. To characterise the surface acidities of the porous aluminas and Pt/Al_2O_3 catalysts, temperature programmed desorption (TPD) with ethanol and *in-situ* diffuse-reflectance infrared spectroscopy (DRIFTS) with CO and pyridine adsorption studies were performed. By comparing with a commercial γ-Al_2O_3 (Puralox) and conventional Pt/Al_2O_3 catalysts prepared by impregnation, the surface properties of the halogen-modified (Cl and F) porous alumina supports and the corresponding Pt/Al_2O_3 NP catalysts were investigated. Through analysis of *n*-hexane reforming at elevated temperatures, the catalytic activity, selectivity, and stability of the Pt/Al_2O_3 catalysts were assessed to understand the conventional bi-functional mechanism for industrial reforming catalysts in terms of new catalytic systems with Pt NPs and well-ordered porous aluminas.

Experimental

Preparation of porous Al_2O_3, Cl-Al_2O_3, and F-Al_2O_3

Porous alumina supports with both macro- and mesopores were synthesised using previously reported methods.[13,34–36] In order to create macropores inside the crystalline alumina walls, polystyrene beads were used a hard template. The polystyrene beads were synthesised via emulsifier-free emulsion polymerisation.[34] Briefly, 14 g of styrene monomer and 0.7 g of divinylbenzene were washed with 0.1 M NaOH solution 4 times and with DI water for additional 4 times to remove the inhibitors. After discarding the bottom layer, the upper organic solution was poured into 140 mL of DI water and maintained at 70 °C with Ar flowing for 1 h. As an initiator, 0.03 g of potassium persulfate dissolved in water was added to the solution. The polymerisation was then allowed to proceed for 12 h at 70 °C, which produced white products. After washing with methanol and water, polystyrene beads with an average diameter of 500 nm were retrieved following centrifugation and drying. Porous aluminas were synthesised by using these polystyrene beads as a macropore template and the Pluronic P123 tri-block copolymer ($(EO)_{20}(PO)_{70}(EO)_{20}$, EO = ethylene oxide, PO = propylene oxide, *M*w = ~ 5,800) as a mesopore template. For this purpose, 4.0 g of Pluronic P123 was completely dissolved in 40 mL of ethanol. The aluminum precursor solution composed of 8.16 g of aluminum isopropoxide (40 mmol, Sigma-Aldrich, >98%) dissolved in 6.4 mL of nitric acid (68–70 wt%) and 20 mL of ethanol was then added into the P123 solution. After reaction for 5 h, 4 g of the polystyrene beads was added to the solution mixture and the ethanol was then slowly evaporated in a petri dish at 60 °C. The resulting flakes were collected and calcined at 900 °C for 10 h in air, which produced highly crystalline γ-Al_2O_3 with average macropore and mesopore sizes of 300 nm and 10 nm, respectively. In order to prepare the chlorinated alumina support (Cl-Al_2O_3),[26,27] as-synthesised porous alumina was mixed with HCl. After drying, the alumina was calcined at 300 °C for 12 h. To prepare the fluorinated alumina support (F-Al_2O_3),[32,33] 0.19 g of NH_4F (Sigma-Aldrich, >98%) dissolved in water was mixed with the porous alumina (4.5 g) and calcined at 550 °C for 5 h.

Preparation of Pt NPs and supported Pt/alumina catalysts

Pt NPs capped by poly(vinylpyrrolidone) (PVP) were synthesised by the polyol reduction method.[13] In particular, 0.04 g of $H_2PtCl_6 \cdot xH_2O$ (0.1 mmol, Sigma-Aldrich, >99.9%) and 0.1 g of PVP were dissolved into 10 mL of ethylene glycol in a 50 mL three-neck round bottom flask. The solution was heated to 50 °C and evacuated at this temperature for 20 min to remove water and oxygen under vigorous magnetic stirring. The flask was then heated to 200 °C and maintained at this temperature for 10 min under an Ar atmosphere. The solution was then cooled to room temperature and an excess of acetone was poured into the solution. The Pt NPs were precipitated by centrifugation and re-dispersed in ethanol. To prepared the supported Pt/alumina catalysts, the porous alumina (either Al_2O_3, Cl-Al_2O_3, or F-Al_2O_3) was added to the Pt NP dispersion. After sonication for 1 h, the precipitates were collected by centrifugation and dried at 90 °C. In order to remove all of the PVP surfactants, the catalysts were washed with acetone and ethanol, and then calcined at 360 °C for 6 h in air.

Characterisation

Transmission electron microscopy (TEM) analysis was conducted using a Hitachi H-7650 instrument operating at 120 kV. X-ray diffraction (XRD) patterns were recorded with a Bruker D4 X-ray diffractometer (Germany) with Ni-filtered Cu Kα radiation (40 kV, 40 mA). Nitrogen adsorption–desorption isotherms were obtained on a Belsorp-max instrument. The Brunauer–Emmett–Teller (BET) method was utilised to calculate the specific surface area (S_{BET}) using adsorption data at p/p_0 = 0.05–0.25. The pore size distribution (PSD) was derived from the adsorption branch by using the Barrett–Joyner–Halenda (BJH) model. Elemental analyses by inductively coupled plasma atomic emission spectroscopy (ICP-OES) were conducted using a Perkin Elmer optical emission spectrometer (Optima 7000 DV). Before the ICP-OES measurements, calibration was conducted using a platinum standard (Fluka, TraceCERT 1000 mg L^{-1}) as a certified reference material (CRM). Thermogravimetric analysis (TGA) was conducted in an air (60 mL/min) and N_2 (40 mL/min) atmosphere in a Pt pan using a TA instrument Q500.

Catalytic reaction

n-Hexane reforming was carried out in a stainless steel tubular plug-flow reactor. The catalysts (0.5–0.7 g) were diluted by quartz and loaded into the reactor bed.[13] The catalyst pre-treatment step consisted of reduction in a 50 vol.% mixture of H_2 and N_2 at a total flow rate of 20 sccm. The reduction treatment was conducted under ambient pressure at 400 °C for 2 h. The *n*-hexane (≥ 99%, Aldrich) vapour was transferred to the reactor by a syringe pump and the reaction was conducted with 140 Torr *n*-hexane and 620 Torr H_2 in the temperature range of 240–400 °C. The reaction products were analysed using an HP 5890 Series II GC equipped with a 10-m dimethylpolysiloxane (HP-1) capillary column in line with a flame ionisation detector (FID).

Ethanol TPD

TPD of ethanol was conducted using a previously described method.[37–39] Before the TPD measurements, the porous alumina was calcined at 500 °C for 1 h under 20% O_2/He at a flow rate of 1.0 mL/s. Then, the alumina was cooled to room temperature and ethanol adsorption was commenced using a 2.0% ethanol/He mixture (1.0 mL/s) for 30 min; He was purged to remove weakly bound ethanol molecules. After stabilisation of the GC FID signal (Agilent 7820A), TPD was carried out using a He flow rate of 1.0 mL/s at a heating rate of 10 °C/min.

DRIFTS

The *in-situ* DRIFTS experiments at low temperature were performed on a Nicolet iS10 FTIR spectrometer equipped with a mercury-cadmium-telluride (MCT) detector to investigate the relative ratio of Lewis to Brønsted acid sites on the alumina surfaces and the Pt NP structure using CO as a probe molecule. All spectra were collected with an average of 128 scans with a resolution of 4 cm^{-1}. Al_2O_3 and the Pt/Al_2O_3 catalysts (12 mg) were loaded into a high temperature reaction chamber (Harrick Scientific) with ZnSe windows, which was installed in a Praying Mantis diffusion reflection accessory. All the samples were pretreated using 20% O_2/He (flow rate = 1 mL/s) at 400 °C for 1 h and then purged with He for 30 min. Reduction of the catalysts was carried out at this temperature using 10% H_2/He for 30 min. Before cooling the samples to 0 °C, the samples were purged with He for 10 min to remove the H_2 on the Pt NPs. CO adsorption was performed on Al_2O_3 and Pt/Al_2O_3 by flowing 0.2% CO/He with repeated pulses (100 μL) at 0 °C. The amount of CO adsorbed on the bare alumina at 0 °C was negligible. After cooling to -150 °C, backgrounds were collected on the catalyst saturated with CO on the Pt surface; the spectra were then collected until there was no change in them under a 0.2% CO/He flow. From this process, the acidic sites of the alumina surfaces were confirmed, where there was no influence of the adsorbed CO on the Pt NPs. The IR spectra collected from the alumina support were normalised with the intensity of the Brønsted acid sites (2154–2158 cm^{-1}). The spectrum with CO adsorbed on the Pt NPs was normalised by the number of CO adsorbed on Pt sites from CO pulse chemisorption, which was separately carried out in a quartz reactor.

Pyridine adsorption

Acid site distributions were also investigated by DRIFTS measurements after pyridine adsorption. All the samples were pretreated as the same protocols described above. Background spectra were collected after cooling the samples to 100 °C, followed by the introduction of 1% pyridine/He for 10 min. The physisorbed pyridine was removed by He purging for 30 min at 100 °C, and the IR spectra were then collected.

Results and Discussion

Structure and morphology

Porous alumina with both macropores and mesopores were synthesised using polystyrene beads as a hard template and P123 tri-block copolymer surfactants as the soft template.[13,34–36] The synthesised porous alumina was treated with HCl or NH_4F to give either chlorinated (Cl–Al_2O_3) or fluorinated (F–Al_2O_3) alumina supports, respectively.[22–33] For the chlorinated alumina, the porous aluminas were treated with HCl vapour followed by calcination at 900 °C for 4 h.[26,27] The chlorine content to the alumina was measured to be ca. 5 wt%. The fluorinated alumina was prepared by mixing 5 g of alumina with 0.16 g of NH_4F dissolved in 20 mL of DI water.[32,33] After drying and calcination at 900 °C for 5 h, F–Al_2O_3 was prepared with a surface fluorine content of 2.5 wt%. To prepare the Pt-supported alumina catalysts, Pt NPs with an average diameter of 2.97 nm were synthesised via the polyol method in the presence of poly(vinylpyrrolidone) (PVP) organic capping molecules and subsequently incorporated into the Cl–Al_2O_3 or F–Al_2O_3 supports via capillary inclusion. The content of Pt NPs to the aluminas was 0.3–0.5 wt%, as measured by inductively coupled plasma atomic emission spectroscopy (ICP-OES). A typical procedure for the preparation of the Pt/Cl–Al_2O_3 catalyst is shown in Fig. 1a. The as-synthesised alumina supports have well-defined macropores and mesopores which were suitable for incorporating colloidal Pt NPs. Images from scanning electron microscopy (SEM, Fig. 1b) and transmission electron microscopy (TEM, Fig. 1c-d) demonstrate that, after calcination at 700 °C, the polystyrene beads (diameter of 500 nm) were successfully eliminated, leaving behind 300 nm sized macropores; the P123 organic surfactants produced small mesopores with an average diameter of 10 nm. TGA results show that Pt supported alumina catalysts suffered weigh loss by removal of PVP (3–5 %), demonstrating that calcination at 360 °C for 6 h in air removed PVP completely (Fig. S2, SI). After chlorination, the porous Cl–Al_2O_3 provided a large surface area to permit homogeneous loading of the Pt NPs, as seen in the TEM image in Fig. 1e.

Crystallinity

XRD patterns show that all the porous oxides have highly crystalline γ-phases, indicating that neither chlorination nor fluorination affected the crystalline structure of porous γ–Al_2O_3 (Fig. S1a of the Supporting Information, SI). The N_2 sorption isotherms of the porous alumina supports show typical type-IV curves with a distinct condensation step and hysteresis loop, which is characteristic of mesoporous structures with a narrow pore size distribution (Fig. S1b, SI). The measured surface areas of the Al_2O_3, Cl–Al_2O_3, and F–Al_2O_3 porous structures were 112, 84, and 111 m^2/g, respectively. Notably, whereas the surfaces area was maintained after fluorination in the F–Al_2O_3 porous structure, Cl–Al_2O_3 showed a reduced surface area compared with unmodified Al_2O_3 (Table S1, SI).

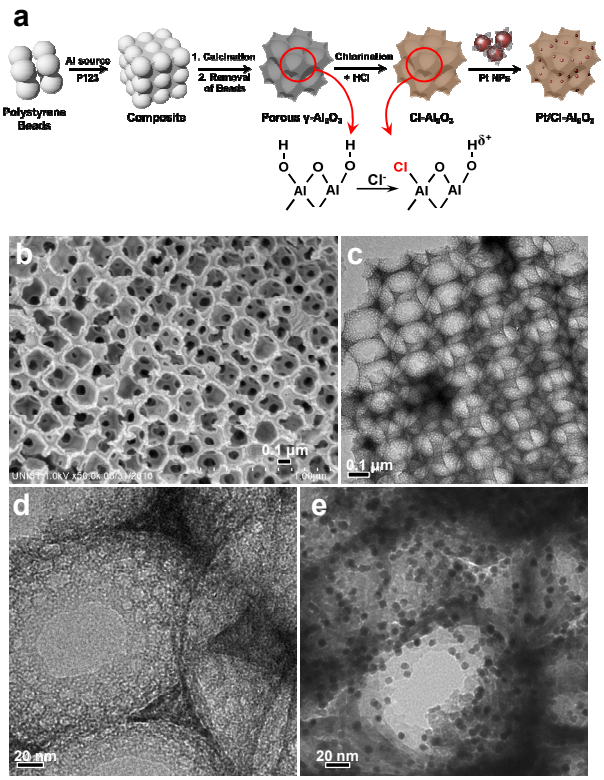

Fig. 1 (a) Synthetic procedure for porous Al_2O_3, Cl–Al_2O_3, and Pt/Cl–Al_2O_3 catalysts. (b) SEM and (c-d) TEM images of porous Al_2O_3 with well-defined macropores and mesopores. (e) TEM image of Pt/Cl–Al_2O_3 catalysts.

n-Hexane Reforming

Subsequently, the catalytic behaviour of the supported Pt/Al_2O_3 catalysts was investigated using the *n*-hexane reforming reaction in a tubular fixed bed reactor with a hexane:H_2 ratio of 1:4.3 at ambient pressure and temperatures ranging from 240 to 400 °C. Further details of this procedure can be found elsewhere.[12–16] Prior to the reaction, all the supported catalysts were pretreated at 400 °C under a gas mixture of N_2 and H_2 (10 sccm) to reduce the Pt surfaces. Fig. 2a shows five major reaction pathways of *n*-hexane reforming. First, *n*-hexane can be converted via skeletal rearrangement to C_6 isomers, including 2-methylpentane (2MP), 3-methylpentane (3MP), and 1,1- and 1,2-dimethylbutane. In terms of producing hydrocarbons with high octane values, branched C_6 isomers are the most desirable products. Second, cyclization of *n*-hexane to methylcyclopentane (MCP) or cyclohexane can occur. Third, the formed cyclohexane can be further dehydrogenated via aromatization to produce benzene. Fourth, olefins such as 1-hexene or methylcyclopentene can be generated via dehydrogenation. Finally, cracked hydrocarbons with less than six carbon atoms can be produced as unwanted products.

Fig. 2b-c show the catalytic activity and product selectivity of the three catalysts with the three types of alumina supports (i.e., Pt/Al_2O_3, Pt/Cl–Al_2O_3, and Pt/F–Al_2O_3). As seen, the reaction rates increased as the reaction temperature

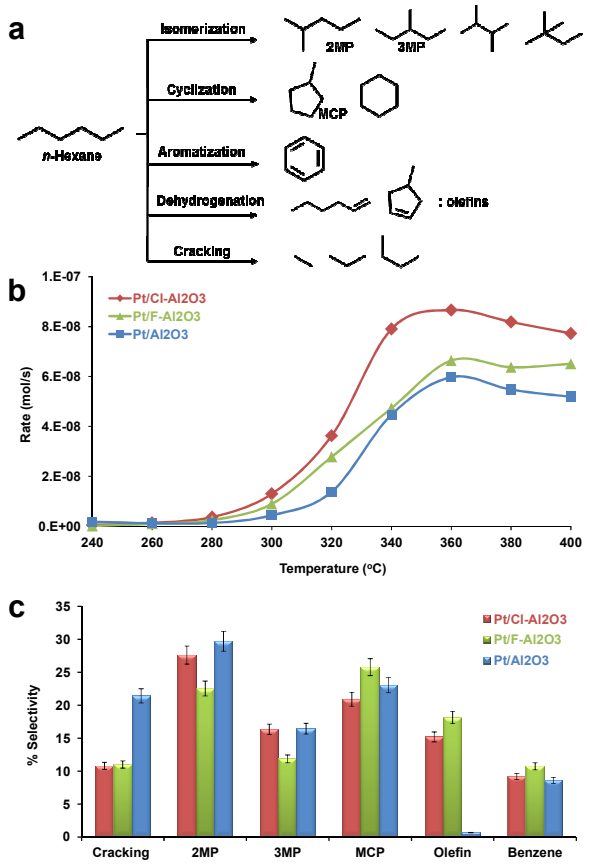

Fig. 2 (a) Possible reaction pathways and products for *n*-hexane reforming. The reaction was performed with a hexane:H_2 ratio of 1:4.3 at temperatures ranging from 240 to 400 °C at ambient pressure. (b) Reaction rates calculated by converting the moles of hexane per second as a function of temperature over the three Pt/Al_2O_3 catalysts. (c) Product selectivity of *n*-hexane reforming measured at 360 °C.

increased, reaching maximum values at 360 °C for all catalysts. These results suggest that catalytic deactivation occurred beyond 360 °C. The origin causing catalyst deactivation will be discussed subsequently. In the meantime, Pt/Cl–Al_2O_3 exhibited the highest reaction rates at all temperatures, followed by Pt/F–Al_2O_3. Full details of the reaction results are summarised in Table S2 of the SI. Fig. 2c compares the product selectivity among the three catalysts. As seen, C_6 isomers including 2MP and 3MP (isomerization) were the major products of the *n*-hexane reforming reaction; MCP (cyclization), benzene (aromatization), olefins (dehydrogenation), and short hydrocarbons (cracking) were also produced at 360 °C. It is noteworthy that Pt/Cl–Al_2O_3 and Pt/F–Al_2O_3 yielded higher olefin levels and fewer cracking products than Pt/Al_2O_3. Furthermore, compared with Pt/F–Al_2O_3, the Pt/Cl–Al_2O_3 catalyst tended to generate a larger number of simple hydrocarbons (i.e. 2MP and 3MP) rather than relatively complex ring hydrocarbons (i.e. MCP and benzene). On the basis of these results, we conclude that Cl–Al_2O_3 and F–Al_2O_3 contain an abundance of acidic sites that facilitated high activity and long-term stability, and suffered less deactivation during the *n*-hexane reforming reaction.

Ethanol TPD

TPD experiments with ethanol were performed in order to characterise the active sites of the Cl–Al_2O_3 and F–Al_2O_3 porous alumina supports.[37–41] Because acidic alumina is a well-known alcohol dehydration catalyst, ethanol TPD is a powerful technique to identify the surface structures and acidic properties of modified alumina supports. It has been reported that γ–Al_2O_3 can thermally transform to the δ–phase, θ–phase, and finally to the α-phase, resulting in different catalytic properties.[37–41] Based on the XRD results, the three porous alumina supports investigated herein (Cl–Al_2O_3, F–Al_2O_3, and unmodified Al_2O_3) exhibited characteristics typical of γ–Al_2O_3 phase (Fig. S1a). As determined in a previous study, α–, γ–, and θ–Al_2O_3 have distinct ethanol TPD profiles; that is, molecularly bound ethanol gives a relatively low temperature peak (<150 °C), whereas ethylene formed by dissociative adsorption of ethanol (ethoxide) and subsequent dehydration on the alumina surface gives a relatively high temperature peak (>150 °C).[37–41] In the present ethanol TPD experiments, the Al^{3+} sites on the (100) facets of γ–Al_2O_3 exhibited an ethylene desorption feature at 217 °C, whereas dissociative adsorption of ethanol on both the Lewis and Brønsted acid sites of the alumina surfaces was indicated at 250 °C, which is a representative property of θ–Al_2O_3.[38] In addition, α-Al_2O_3 showed a broad ethylene desorption around 320 °C. Note that Puralox SBA-200 (Sasol) was used in the ethanol TPD experiments as a pure γ–Al_2O_3 reference. Fig. 3 shows a typical ethanol TPD profile of γ–Al_2O_3 (Puralox) with a strong ethylene desorption peak at 225 °C. The ethanol TPD profiles of the porous alumina supports examined herein (i.e. Al_2O_3, Cl–Al_2O_3, and F–Al_2O_3) have broad peaks at 70 °C and approximately 300 °C. These results indicate that the surface acidic properties of Al_2O_3, Cl–Al_2O_3, and F–Al_2O_3 are similar to α–Al_2O_3, even though the XRD measurements suggest that the porous alumina crystal structures correspond to the γ-phase. When the peak profiles around 300 °C are enlarged (Fig. 3, inset), it is clear that the desorption temperatures (T_d) of both Cl–Al_2O_3 and F–Al_2O_3 are lower than the original porous Al_2O_3. Notably, the surface acidities of Cl–Al_2O_3 and F–Al_2O_3 are enhanced

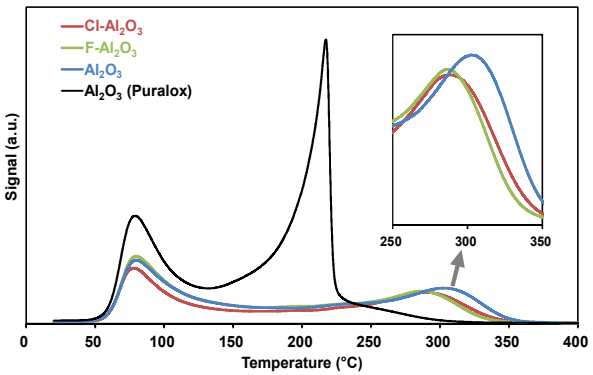

Fig. 3 TPD profiles after ethanol adsorption on different alumina supports (inset: TPD profiles of Al_2O_3, Cl–Al_2O_3, and F–Al_2O_3 are highlighted). A commercial γ–Al_2O_3 (Puralox) was measured as a reference.

relative to the original porous Al_2O_3, as evidenced by their lower T_d values (303 °C for Al_2O_3 versus 287 °C for Cl–Al_2O_3 and F–Al_2O_3).

In-situ DRIFTS

Low temperature *in-situ* DRIFTS experiments with CO adsorption were also performed to study the surface properties of the Cl– and F–modified alumina supports. It has previously been reported that CO molecules interact with both Lewis and Brønsted acid sites on alumina surfaces.[42] As seen in Fig. 4, the IR spectra collected from the alumina supports after CO adsorption showed two distinctive bands: a high-frequency peak at 2194–2186 cm^{-1}, which is assigned to CO adsorption on the Lewis acid sites; and a low frequency peak at 2158–2155 cm^{-1}, which is assigned to CO adsorption on the Brønsted acid sites.[42,43] In order to compare the relative ratio of Lewis to Brønsted acid sites, each spectrum was normalised by the Brønsted site intensity of the 2156 cm^{-1} band. In Fig. 4a, the relative ratio of Lewis to Brønsted acid sites were found to vary in Cl–Al_2O_3, F–Al_2O_3, and Al_2O_3 as 0.64, 0.54, and 0.56, respectively.

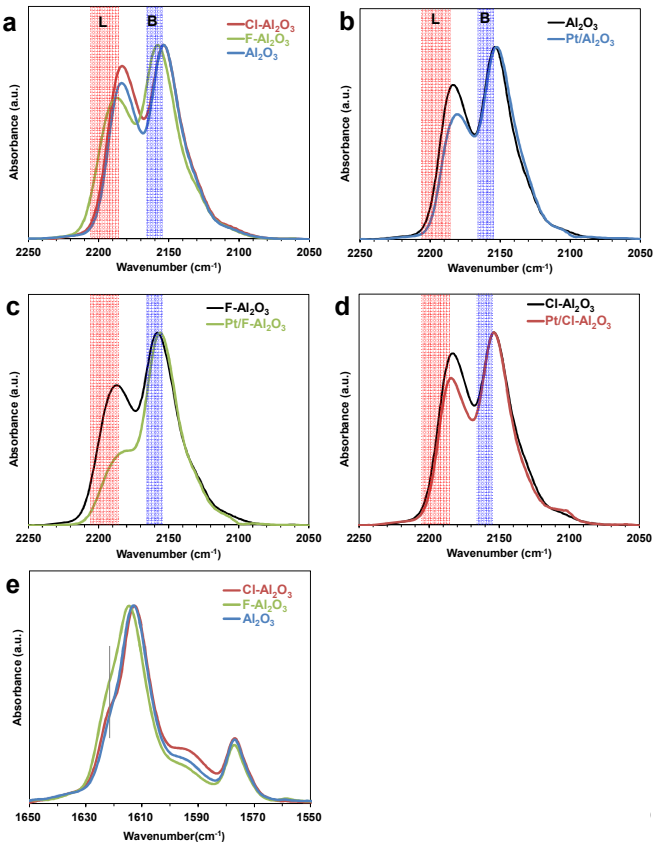

Fig. 4 *In-situ* DRIFT spectra after CO adsorption at -150 °C on (a) porous alumina supports and (b-d) their corresponding Pt/alumina catalysts. The Lewis acid (L) and Brønsted (B) sites are clearly distinguished at 2194–2186 and 2158–2155 cm^{-1}, respectively. (e) *In-situ* DRIFT spectra after pyridine adsorption at 100 °C on porous aluminas.

Notably, the maxima vibrational frequency peaks in Cl–Al_2O_3 were identical to the analogous peaks in Al_2O_3 without acid modification; however, both vibrational peaks of F–Al_2O_3 were shifted to higher frequencies, indicating a change of the acid site strength (Fig. 4a). We also compared the change in the IR spectra after Pt loading onto the alumina supports (Fig. 4b-d). In all three Pt/alumina catalysts, the relative intensities of CO on the Lewis acid sites decreased significantly after Pt loading, whereas the Brønsted site showed the same intensity as the original alumina support. We also carried out *in-situ* DRIFTS experiments with pyridine adsorption at 100 °C (Fig. 4e). The absorption peaks were clearly distinguished at 1612 and 1621 cm^{-1}, which correspond to the adsorption of pyridine to Al–OH and Al^{3+} sites of the alumina surfaces, respectively.[44–46] When the spectrum was normalised by the 1612 cm^{-1} peak, the relative ratios of Lewis to Brønsted acid sites of Cl–Al_2O_3 and F–Al_2O_3 were further increased than the original Al_2O_3. It is also confirmed that the peak shift of F–Al_2O_3 moved toward higher frequency, which was also found in the DRIFTS by CO adsorption (Fig. 4e). Based on these results, we concluded that Pt NPs were preferentially deposited to the Lewis acid sites of the alumina supports.

In-situ DRIFTS experiments with CO adsorption can also be used to predict the geometric and electronic properties of the Pt NPs. The IR spectrum of CO on the Pt/γ-Al_2O_3 catalyst (5 wt% Pt) prepared by a conventional impregnation method exhibited broad bands in the region of 2000–2120 cm^{-1}, indicating the presence of various under-coordinated CO adsorption sites on the Pt NPs (Fig. 5, inset). The adsorption features of CO on supported Pt catalysts in IR spectra are well understood and reported.[47–51] In the range of 2000–2100 cm^{-1}, a peak near 2090 cm^{-1} was assigned to CO linearly bound to well-coordinated sites (terrace) of Pt (111) facets, while the low-frequency region at 2060–2090 cm^{-1} indicated that CO was linearly bound to under-coordinated sites (i.e. step, edge, and corner).[47–51]

Due to the small number and dispersed nature of the Pt species of the Pt/γ–Al_2O_3 catalyst by the impregnation method, broad bands in the region of under-coordinated sites were exhibited (Fig. 5). However, in the modified Pt/Al_2O_3 samples, only one narrow peak at 2096 cm^{-1} was present, because CO was linearly adsorbed onto well-coordinated terrace sites of the Pt (111) facet due to the size of Pt NPs.[47,52,53] The IR adsorption spectra at 1500–1900 cm^{-1} contained 2- and 3-fold bridged sites of CO on Pt and the region at 1200–1650 cm^{-1} indicated distinct carbonate features of. On the basis of these results, we conclude that the Pt (111) NPs prefer to be deposited on the Lewis acid sites of the porous alumina supports.

Thermal stability

To confirm the thermal stability of the Pt/Al_2O_3 catalysts, the *n*-hexane reforming reaction was carried out at 400 °C for 48 h, because severe deactivation occurred beyond 360 °C. Before reaction, the surface of the Pt NPs was reduced by H_2 at 400 °C for 2 h. Fig. 6a shows that the average size of the Pt NPs

in Pt/Al_2O_3 after H_2 reduction at 400 °C was 6.11 nm. Compared with the as-synthesised Pt NPs (2.97 nm), the size of Pt in Pt/Al_2O_3 increased after reduction as a result of thermal aggregation. After *n*-hexane reforming at 400 °C for 48 h, the size of Pt NPs was further increased to 9.94, 8.02, and 7.77 nm for Pt/Al_2O_3, $Pt/Cl\text{-}Al_2O_3$, and $Pt/F\text{-}Al_2O_3$, respectively (Fig. 6b-d). Although the $Pt/Cl\text{-}Al_2O_3$ catalysts exhibited less aggregation than the others, the aggregation behaviour was similar for the three catalysts.

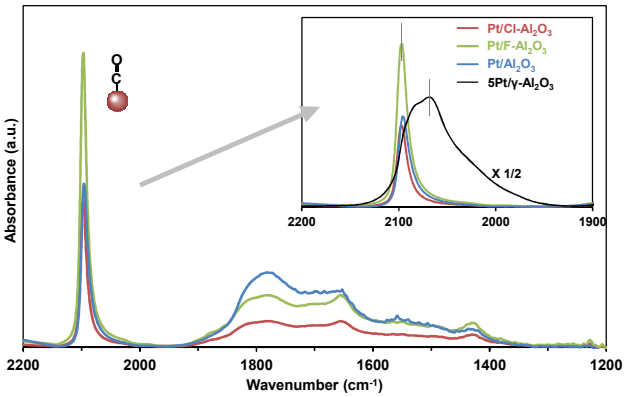

Fig. 5 CO adsorption spectra of Pt/alumina catalysts at 0 °C, which were normalized by CO adsorption of CO-TPD (inset: The spectra at the region of 1900 - 2000 cm^{-1} are highlighted). The CO vibration frequency at 2100 cm^{-1} on Pt corresponds to linearly adsorbed CO on the terrace sites of the Pt (111) facet.

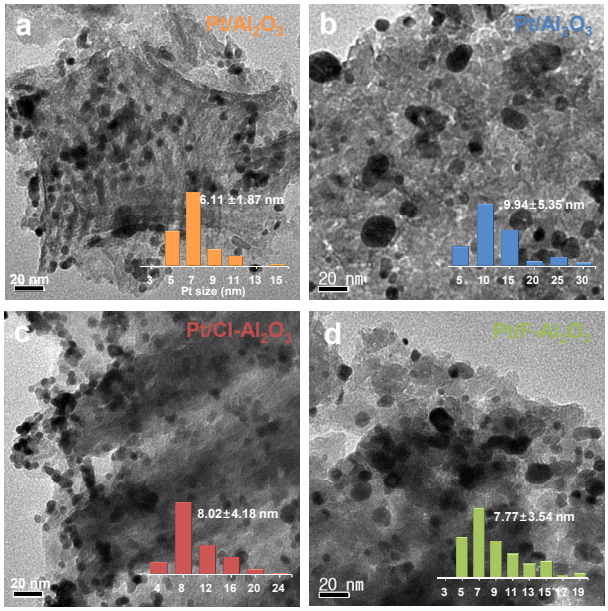

Fig. 6 TEM images of Pt/Al_2O_3 catalysts before and after *n*-hexane reforming at 400 °C and the corresponding Pt particle size histograms: (a) H_2 treated Pt/Al_2O_3 catalysts at 400 °C before *n*-hexane reforming, (b) Pt/Al_2O_3, (c) $Pt/Cl\text{-}Al_2O_3$, (d) $Pt/F\text{-}Al_2O_3$ catalysts after *n*-hexane reforming at 400 °C for 48 h.

We compared the weight loss of spent catalysts by TGA to measure the amount of coke generated. The degree of carbon weight loss of Pt/Al_2O_3, $Pt/Cl\text{-}Al_2O_3$, and $Pt/F\text{-}Al_2O_3$ was 5.3, 2.9, and 3.9 %, respectively (Fig. S3, SI). Considering the total weight of the samples measured, the amount of coke produced by the reaction shows a marked difference among the catalysts. During *n*-hexane reforming at 400 °C, the reaction rate remained steady for 48 h (Fig. S4, SI). From these results, it is clear that the origin of catalyst deactivation can be attributed to coking rather than Pt sintering during high temperature reforming. $Pt/Cl\text{-}Al_2O_3$ experienced less deactivation than the other catalysts due to the presence of its $Cl\text{-}Al_2O_3$ support.

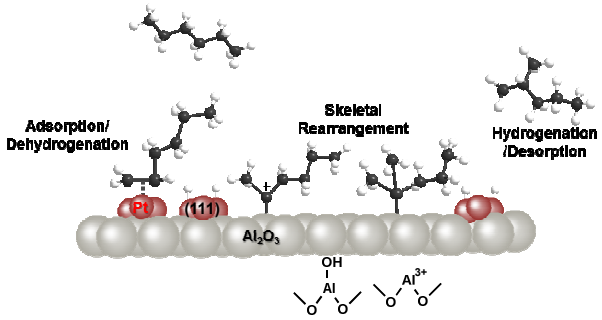

Scheme 1 Schematic representation of the bi-functional mechanism of *n*-hexane reforming on alumina-supported Pt catalysts.

Bi-functional mechanism

Based on the investigations by *in-situ* DRIFTS with CO adsorption, the current Pt/Al_2O_3 catalysts composed of colloidal Pt NPs and ordered porous alumina with well-defined structures have totally different adsorption behaviours than are demonstrated with conventional impregnated Pt/Al_2O_3 catalysts. In particular, the contact between Pt and Al_2O_3 in the current Pt/Al_2O_3 catalysts is relatively poor, due to the additional incorporation step of Pt into the alumina and the existence of organic surfactants. Nevertheless, this new type of Pt/Al_2O_3 nanocatalysts provides additional insight for understanding the bi-functional mechanism of *n*-hexane reforming. In particular, the well-defined Lewis acid sites of $Cl\text{-}Al_2O_3$ resulted in higher catalytic activity than $F\text{-}Al_2O_3$ and Al_2O_3. The enhanced acidity of $Pt/Cl\text{-}Al_2O_3$, as confirmed by the CO chemisorption experiments, modified the hydrocarbon skeletal rearrangements by preferentially generating C_6-branched products via an acid-catalysed mechanism. The traditional bi-functional mechanism of reforming over Pt/Al_2O_3 catalysts indicates that Lewis acid sites stabilise intermediate carbocation species to promote the production of isomers, which is accompanied by dehydrogenation/hydrogenation steps involving the Pt metal (Scheme 1).[14,54–58] It was previously reported that mesoporous zeolites with very strong Brønsted sites favour cracking via β-scission.[12] However, Al-modified mesoporous silica supports with a moderate concentration of Lewis and Brønsted acid sites induced high isomerization selectivity.[14,59] Similarly, due to the enhancement of the Lewis acid sites in the $Cl\text{-}Al_2O_3$ alumina support prepared in this work, the activity of the *n*-hexane reforming reaction was increased greatly, with the selectivity

favouring highly branched isomers with minimal cracking. Although Pt became aggregated during the high temperature reforming of *n*-hexane, the Pt/Cl-Al_2O_3 catalysts suffered less coking than the Pt/Al_2O_3 and Pt/F-Al_2O_3 catalysts. Overall, the combined studies confirmed that chlorinated alumina plays an important role for Pt/Al_2O_3 catalysts, resulting in a limited amount of coking during the high temperature reforming process, thereby retarding Pt deactivation and resulting in longer periods of high catalytic activity.[60,61]

Conclusions

Porous alumina supports were modified by chlorination and fluorination to enhance their resultant surface acidity. The resultant porous alumina supports with well-defined macropores and mesopores were used to prepare alumina-supported Pt NP catalysts (i.e. Pt/Al_2O_3, Pt/Cl-Al_2O_3, and Pt/F-Al_2O_3). The catalytic activities of these catalysts were assessed in terms of the *n*-hexane reforming reaction. Compared with Pt/Al_2O_3, the modified Pt/Cl-Al_2O_3 and Pt/F-Al_2O_3 catalysts exhibited enhanced activity as well as higher olefin levels and less cracking. Similarly, the ethanol TPD experiments revealed that the surface acidities of Cl-Al_2O_3 and F-Al_2O_3 were enhanced relative to Pt/Al_2O_3. *In-situ* DRIFTS experiments with CO and pyridine adsorption demonstrated the relative ratio of Lewis to Brønsted acid sites was increased in Cl-Al_2O_3 relative to F-Al_2O_3 and Pt/Al_2O_3. The experiments also confirmed that Pt NPs with (111) facets preferentially occupied the Lewis acid sites of the porous alumina supports in the Pt/Al_2O_3 catalysts. Taken together, the results demonstrate that the enhancement of the Lewis acid sites in Cl-Al_2O_3 induced high reaction rates of *n*-hexane reforming with less coking over all temperature ranges investigated, with catalytic behaviours in accordance with the well-known bi-functional mechanism of reforming processes. Additionally, the results demonstrate how newly developed NP-based catalysts are designed, characterised, and verified for comparison with conventional reforming catalysts. With robust and well-defined pore structures and Lewis acid sites, porous chlorinated alumina is an effective support for Pt catalysts in *n*-hexane reforming.

Conflicts of interest

There are no conflicts to declare.

Acknowledgements

This research was supported by Basic Science Research Program through the National Research Foundation of Korea (NRF) funded by the Ministry of Education (2015R1C1A1A01055092, 2016R1A5A1009405, and 2017R1A2B4007310) and C1 Gas Refinery Program through the NRF funded by the Ministry of Science, ICT & Future Planning (2015M3D3A1A01064899). G.A.S thanks for the support by the Director, Office of Science, Office of Basic Energy Sciences, Division of Chemical Sciences, Geological and Biosciences of the US Department of Energy under Contract Number DEAC02-05CH11231.

References

1 J. Hagen in *Industrial Catalysis: A Practical Approach*, 2nd edition, Wiley-VCH, Weinheim, 2006.
2 G. Alfke, W.W. Irion and O.S. Neuwirth in *Oil Refining, Ullman's Encyclopedia of Industrial Chemistry*, Wiley-VCH, Weinheim, **2007**.
3 G. A. Somorjai in *Introduction to Surface Chemistry and Catalysis*; Wiley: New York, 2010.
4 J. W. Geus and J.A.R van Ween, in *Catalysis: An Integrated Approach to Homogeneous, Heterogeneous and Industrial Catalysis*, Vol. 79 (Eds.: Moulijn, J.A.; van Leeuwen, P.W.N.M.; van Santen, R.A.), Elsevier, Amsterdam, **1993**.
5 E. Christoffel, F. Fetting and H. Vierrath, *J. Catal*. 1975, **40**, 349-355.
6 I. Surjo and E. Christoffel, *J. Catal.* 1979, **60**, 133-139.
7 T. N. Vu, J. van Gestel, J. P. Gilson, C. Collet, J. P. Dath and J. C. Duchet, *J. Catal*. 2005, **231**, 453-467.
8 J. Y. Park in *Current Trends of Surface Science and Catalysis*, Springer, 2016.
9 G. A. Somorjai and J. Y. Park, *Angew. Chem. Int. Ed*. 2008, **47**, 9212-9228.
10 S. M. Davis, F. Zaera and G. A. Somorjai, *J. Catal.* 1984, **85**, 206-223.
11 K. An and G. A. Somorjai, *ChemCatChem* 2012, **4**, 1512-1524.
12 N. Musselwhite, S. Alayoglu, G. Melaet, V. V. Pushkarev, A. E. Lindeman, K. An and G. A. Somorjai, *Catal. Lett*. 2013, **143**, 907-911.
13 K. An, S. Alayoglu, N. Musselwhite, K. Na and G. A. Somorjai, *J. Am. Chem. Soc*. 2014, **136**, 6830-6833.
14 N. Musselwhite, K. Na, S. Alayoglu and G. A. Somorjai, *J. Am. Chem. Soc.* 2014, **136**, 16661-16665.
15 N. Musselwhite, K. Na, K. Sabyrov, S. Aayogu and G. A. Somorjai, *J. Am. Chem. Soc*. 2015, **137**, 10231-10237.
16 K. An, Q. Zhang, S. Alayoglu, N. Musselwhite, J. Y. Shin and G. A. Somorjai, *Nano Lett.* 2014, **14**, 4907-4912.
17 M. P. González-Marcos, B. Iñarra, J. M. Guil and M. A. Gutiérrez-Ortiz, *Catal. Today* 2005, **107**, 685-692.
18 F. M. Dautzenberg, J. N. Helle, P. Biloen and W. M. H. Sachtler, *J. Catal.* 1980, **63**, 119-128.
19 R. Burch and L. C. Garla, *J. Catal*. 1981, **71**, 360-372.
20 S. R. Bare, F. D. Vila, M. E. Charochak, S. Prabhakar, W. J. Bradley, C. Jaye, D. A. Fischer, S. T. Hayashi, S. A. Bradley and J. J. Rehr, *ACS Catal.* 2017, **7**, 1452-1461.
21 I. Contreras-Andrade, A. Vázquez-Zavala and T. Viveros, *Energ. Fuel*. 2009, **23**, 3835-3841.
22 P. O. Scokart, S. A. Selim, J. P. Damon and P. G. Rouxhet, *J. Colloid. Interf. Sci.* 1979, **70**, 209-222.
23 G. Clet, J. M. Goupil, G. Szabo and D. Cornet, *Appl. Catal. a-Gen.* 2000, **202**, 37-47.
24 A. Melchor, E. Garbowski, M. V. Mathieu and M. Primet, *J. Chem. Soc. Farad. T.* 1986, **82**, 1893-1901.
25 P. M. Bernard and M. Primet, *J. Chem. Soc. Farad. T*. 1990, **86**, 567-570.
26 T. X. Cai, J. P. Qu, S. Q. Wong, Z. Y. Song and H. Min, *Appl. Catal. a-Gen*. 1993, **97**, 113-122.
27 A. G. Gayubo, F. J. Llorens, E. A. Cepeda and J. Bilbao, *Ind. Eng. Chem. Res*. 1997, **36**, 5189-5195.
28 H. Shi, O. Y. Gutierrez, H. Yang, N. D. Browning, G. L. Haller and J. A. Lercher, *ACS Catal*. 2013, **3**, 328-338.
29 W. K. Hall, F. E. Lutinski and H. R. Gerberich, *J. Catal*. 1964, **3**, 512-527.
30 J. W. Hightower, H. R. Gerberic and W. K. Hall, *J. Catal*. 1967, **7**, 57-67.

31 A. Corma, V. Fornes and E. Ortega, *J. Catal*. 1985, **92**, 284-290.
32 A. Corma and V. Fornes, *Appl. Catal*. 1990, **61**, 175-185.
33 L. M. Rodriguez, J. Alcaraz, M. Hernandez, M. Dufaux, Y. Ben Taarit and M. Vrinat, *Appl. Catal. a-Gen.* 1999, **189**, 53-61.
34 J. P. Dacquin, J. Dhainaut, D. Duprez, S. Royer, A. F. Lee and K. Wilson, *J. Am. Chem. Soc*. 2009, **131**, 12896-12897.
35 B. T. Holland, C. F. Blanford and A. Stein, *Science* 1998, **281**, 538-540.
36 A. Stein, *Micropor. Mesopor. Mat*. 2001, **44**, 227-239.
37 J. Lee, E. J. Jang and J. H. Kwak, *J. Catal*. 2017, **345**, 135-148.
38 J. H. Kwak, C. H. F. Peden and J. Szanyi, *J. Phys. Chem. C* 2011, **115**, 12575-12579.
39 J. H. Kwak, J. Lee, J. Szanyi and C. H. F. Peden, *Catal. Today* 2016, **265**, 240-244.
40 J. H. Kwak, D. H. Mei, C. H. F. Peden, R. Rousseau and J. Szanyi, *Catal. Lett*. 2011, **141**, 649-655.
41 J. H. Kwak, J. Z. Hu, A. Lukaski, D. H. Kim, J. Szanyi and C. H. F. Peden, *J. Phys. Chem. C* 2008, **112**, 9486-9492.
42 J. Szanyi and J. H. Kwak, *Phys. Chem. Chem. Phys.* 2014, **16**, 15117-15125.
43 C. Morterra and G. Magnacca, *Catal. Today* 1996, **27**, 497-532.
44 A. Platon and W. J. Thomson, *Ind. Eng. Chem. Res*. 2003, **42**, 5988-5992.
45 F. Abbattista, S. Delmastro, G. Gozzelino, D. Mazza, M. Vallino, G. Busca, V. Lorenzelli and G. Ramis, *J. Catal*. 1989, **117**, 42-51.
46 T. Kawai, K. M. Jiang and T. Ishikawa, *J. Catal*. 1996, **159**, 288-295.
47 Y. J. Zhu and F. Zaera, *Catal. Sci. Technol*. 2014, **4**, 955-962.
48 M. J. Kale and P. Christopher, *ACS Catal*. 2016, **6**, 5599-5609.
49 J. Szanyi and J. H. Kwak, *Phys. Chem. Chem. Phys*. 2014, **16**, 15126-15138.
50 P. Hollins, *Surf. Sci. Rep*. 1992, **16**, 51-94.
51 K. Ding, A. Gulec, A. M. Johnson, N. M. Schweitzer, G. D. Stucky, L. D. Marks and P. C. Stair, *Science* 2015, **350**, 189-192.
52 N. Sheppard and C. De La Cruz, *Catal. Today* 2001, **70**, 3-13.
53 A. D. Allian, K. Takanabe, K. L. Fujdala, X. Hao, T. J. Truex, J. Cai, C. Buda, M. Neurock and E. Iglesia, *J. Am. Chem. Soc*. 2011, **133**, 4498-4517.
54 J. Fung and I. Wang, *J. Catal*. 1996, **164**, 166-172.
55 S. Triwahyono, A. A. Jalil, N. N. Ruslan and N. H. N. Kamarudin, *J. Catal*. 2013, **303**, 50-59.
56 S. Ramirez, M. Viniegra, J. M. Dominguez, P. Schacht and L. C. DeMenorval, *Catal. Lett*. 2000, **66**, 25-32.
57 G. M. Pajonk, *Appl. Catal. a-Gen*. 2000, **202**, 157-169.
58 F. Roessner, U. Roland and *J. Mol. Catal. A: Chem*. 1996, **112**, 401-412.
59 B. Ducourty, G. Szabo, J. P. Dath, J. P. Gilson, J. M. Goupil and D. Cornet, *Appl. Catal. a-Gen*. 2004, **269**, 203-214.
60 C. H. Bartholomew, *Catal. a-Gen*. 2001, **212**, 17-60.
61 S. R. Bare, F. D. Vila, M. E. Charochak, S. Prabhakar, W. J. Bradley, C. Jaye, D. A. Fischer, S. T. Hayashi, S. A. Bradley and J. J. Rehr, *ACS Catal*. 2017, **7**, 1452-1461.

Journal Name

ARTICLE

Graphical Abstract

Catalytic activity and selectivity of *n*-hexane reforming are changed significantly by surface acidic properties of the alumina support following halogen treatment.